Mapping vesicle dynamics onto that of a rigid sphere in five dimensions

A. Aarab,[1] M. Guedda,[2] N. Alaa,[1] and C. Misbah[3,*]

[1]*LAMAI, Département de Mathématiques, FST Gueliz Université de Cady Ayyad, 40000 Marrakech, Morocco*
[2]*LAMFA, CNRS UMR 7352, Département de Mathématiques Université de Picardie Jules Verne, Amiens, France*
[3]*LIPhy, CNRS UMR 5588, Laboratoire Interdisciplinaire de Physique, Université Grenoble, Grenoble, France*

(Received 10 June 2018; revised manuscript received 22 August 2018; published 11 October 2018)

Vesicles are sacs made of a phospholipid bilayer, and they mimic the cytoplasmic membrane of real cells, for which red blood cells constitute a canonical example. Vesicles deform under flow, such as a shear flow. Under a linear shear flow, they are known to exhibit several motions that combine orientation and shape deformation (such as tank treading, vacillating breathing, and so on). It is shown here that the equations of motion of a vesicle under shear flow in the weak deformation regime can be mapped onto those of a loaded (or heavy bottom) rigid sphere in five dimensions in fictitious gravitational and shear fields. Based on our previous exact analytical solutions for vesicles (which we extend here to out-of-shear-plane motions), we provide hitherto unrevealed exact explicit solution for the rigid sphere problem. We explain how deformation of a vesicle in real space can be extracted from a rigid body dynamics in five dimensions upon appropriate projection onto a lower dimension. This study offers a framework where rigid spheres and deformable vesicles are recast into the same universality class in which both systems are described by the same formal equations differing only by the space dimension.

DOI: 10.1103/PhysRevE.98.042407

I. INTRODUCTION

A vesicle (a simple model for red blood cell), which is a closed membrane suspended in an aqueous medium, has received increasing attention from various viewpoints of nonequilibrium sciences due to its relevance to real biological cells [1]. Vesicle dynamics under flow has revealed a large variety of motions that combine orientation and shape deformation, which impact on the suspension rheological behavior [1–4]. In its full generality, this problem is complex due to the free-boundary character of the vesicles. The shape, which changes in time, results from an interplay between the local flow and interfacial forces leading to nonlocal and nonlinear equations. In a general flow and for arbitrary shape deformation, the full evolution equations are intractable analytically. However, in certain asymptotic limits, to be discussed below, the dynamics can be simplified.

When subject to a linear shear flow $\mathbf{u}_0 = (\dot{\gamma} y, 0, 0)$, where $\dot{\gamma}$ is the shear rate, vesicles, which represent the simplest model of an individual red blood cell (RBC), exhibit a variety of different regimes of motion depending on three physical parameters (see for example [5–24]): (i) the excess area $\Delta = (A - 4\pi r_0^2)/r_0^2$, where A is the vesicle area and $r_0 = (3V/4\pi)^{1/3}$ is the effective vesicle radius defined via its volume V, (ii) the viscosity contrast $\lambda = \eta_{\rm int}/\eta_{\rm ext}$, where $\eta_{\rm int}$ and $\eta_{\rm ext}$ are the viscosities of the internal and the external fluids, respectively, and (iii) the so-called capillary number (in analogy with drops) measuring the flow strength over the bending energy of the membrane; $\mathcal{C}_\kappa = \eta_{\rm ext}\dot{\gamma} r_0^3/\kappa$, with κ being the membrane bending rigidity modulus.

Theoretical models and numerical simulations predict three basic types of dynamical regimes in which the viscosity contrast plays a crucial role (see for example [12,25]): tank-treading (TT) mode for small enough λ, in which the vesicle deforms into a prolate ellipsoid inclined at a stationary angle $\psi < \pi/4$ with the flow direction, tumbling (TB) mode for large λ, in which the membrane flips like a rigid body, and vacillating-breathing (VB) mode in which the main axis of the vesicle oscillates about the flow direction, but does not perform full rotations (the inclination angle ψ oscillates around 0 in the interval $[-\pi/4, \pi/4]$), whereas its shape undergoes a breathing motion. Sometimes, the VB mode, which occurs for intermediate values of λ, is called trembling or swinging observed for RBC and is seen as an intermediate regime between TT and TB [26–28]. There is also another regime known as kayaking (K) (a denomination already used before for rigid particles, polymers, liquid crystals). In this regime, the main axis of the vesicle traces a cone outside the shear plane [22]. For rigid ellipsoids, this motion was described by Jeffery [29]; the main axis describes a cone about the perpendicular to the plane of the shear flow. In [30], it is indicated that the K regime describes a component of tumbling motion (out of the shear plane) in which the vesicle's motion possesses a "spin" like the paddle of a kayak.

The TT and TB regimes and the transition between them are well described by the Keller-Skalak (KS) theory [5] in which the vesicle has a fixed shape. KS showed that more viscous particles (i.e., large λ) tumble while less viscous (i.e., small λ) tank tread.

The dynamical regime of VB was discovered in 2006 [12] (see also [15,18,25]). Although the determination of the vesicle shapes is very complex, the physical origin of VB mode is explained analytically by a simple argument [12]. The idea is based on the small deformation approach in which the vesicle

*Corresponding author: chaouqi.misbah@univ-grenoble-alpes.fr

shape is close to a sphere. In that work it was shown that the reductive perturbation method is possible and resulted into a simple model which described successfully the VB mode in addition to the classical TT and TB regimes. More precisely, it is found that a quasispherical vesicle (i.e., Δ is small) exhibits TT for small enough λ. Upon increasing λ the TT regime loses its stability in favor of the VB or the TB regimes (depending on initial conditions). Subsequent analytical extensions of this work have been given [16,17,31] and systematic numerical simulations have been performed [22,23]. The theory presented in [31] has provided a very good agreement with full simulations (see also [22] for a direct comparison between theory and simulations).

In the small deformation theory (or the lowest order of a perturbation theory), the deviation of the shape from a sphere is parametrized by ($r_0 = 1$, or in other words lengths are measured in unit of r_0)

$$r = 1 + \sum_{|m|\leqslant 2} F_{2m}\mathcal{Y}_{2m}, \tag{1}$$

where $\mathcal{Y}_{2m}$, $|m| = 0, 1, 2$, are the usual spherical harmonics of order two. Note that for a quasispherical shape F_{1m} can be set to zero since it corresponds to a solid translation. F_{2m} are unknown time-dependent coefficients satisfying the constraint of fixed total area

$$\frac{\Delta}{2} = \sum_{|m|\leqslant 2} |F_{2m}|^2. \tag{2}$$

The evolution equations for F_{2m} are given by [3]

$$\frac{dF_{2m}}{dt} = \dot{\gamma}\left\{-i\frac{m}{2}\delta_{2|m|}h + i\frac{m}{2}F_{2m} - h\sqrt{\frac{6}{5\pi}}\mathcal{C}_\kappa^{-1}(6+\sigma_0)F_{2m}\right\}, \tag{3}$$

where $i^2 = -1$, $|m| \leqslant 2$, $h = 60\sqrt{2\pi/15}/(32 + 23\lambda)$, and σ_0 is the isotropic part of the tension (or a Lagrange multiplier).

The constraint of fixed total area leads to

$$\sigma_0 = -6 + i\mathcal{C}_\kappa\Delta^{-1}\sqrt{\frac{10\pi}{3}}(F_{22} - F_{2-2}). \tag{4}$$

Therefore, Eq. (3) reads as

$$\frac{dF_{2m}}{dt} = \dot{\gamma}\left\{-i\frac{m}{2}\delta_{2|m|}h + i\frac{m}{2}F_{2m} + \frac{4h}{\Delta}\mathrm{Im}(F_{22})F_{2m}\right\}, \tag{5}$$

which is independent of the bending number $\mathcal{C}_\kappa$. This is the main evolution equation for the quasispherical vesicle shape to the leading order [12,32].

The evolution in time of the vesicle shape configuration in the shear plane is given by the dynamics of F_{22}. $F_{2\pm1}$ and F_{20} modes describe deformations out of the shear plane (see also [15] for more details). More precisely, the out-of-plane deformation along the vorticity direction is described by the F_{20} mode. Usually, $F_{2\pm1}$ modes are ignored for simplicity. In this case, it is shown that the three classical regimes (TT, TB, and VB) are qualitatively described by a two-dimensional model [12] satisfied by $\mathcal{R}$ and ψ, which are defined by $F_{22} = \sqrt{\Delta}/2\mathcal{R}e^{-2i\psi}$. The orientation angle ψ coincides with the inclination angle of the long axis (with respect to the flow direction) of the vesicle in the flow and $\mathcal{R}$ is the amplitude of deformation of the vesicle. This quantity measures the ellipticity of the vesicle contour in the shear plane.

The initial motivation of this work is to reexamine in detail Eq. (5) by including $F_{2\pm1}$ modes. In particular, we have formulated the following questions: If initially the vesicle is placed out of the shear plane, how does the vesicle behave relative to the three classical regimes? Can we obtain explicit analytical expressions of F_{2m} modes, where $|m| \leqslant 2$, and in a simple manner as in Ref. [24] (see below)?

It should be mentioned that Biben *et al.* [22] have reported on simulation results of off-shear plane motions for vesicles for different values of the viscosity contrast and the bending number. It is found that K mode appears when the viscosity contrast and the bending number are both high enough. More importantly, it is shown that K mode seems to occur even if the vesicle is initially forced to be in the shear plane.

This paper attempts to address the above questions at low deformability. During our theoretical investigation, we unexpectedly found that a deformable vesicle can be mapped into a heavy bottom rigid sphere (or loaded sphere, in the sense that the geometrical center of the sphere does not coincide with the mass center) problem in five dimensions. In other words, both (deformable) vesicles and rigid spherical particles satisfy formally the same equations provided the rigid sphere problem is defined in higher dimensions. This will constitute the main focus of this paper. This is interesting in as much as dynamics of rigid and deformable particles can be both recast into the same formal equation. Furthermore, taking into consideration the fact that the vesicle problem (when $F_{21} = 0$) has been shown to have an exact analytical solution [24], the mapping will allow to provide an explicit exact solution for the loaded sphere problem. We will also extend our original solution to the case where $F_{21} \neq 0$. The loaded rigid sphere problem has appeared in the literature in different contexts. It has been analyzed in the context of gyrotaxis or magnetotaxis [33,34] (see below), as well as in the context of swimming of microorganisms [35]. It will be seen here that our mapping and the availability of an exact solution offers some interesting perspectives to study swimming in external flow field. We will briefly comment on the idea that in a Poiseuille flow a swimming loaded sphere can move away from the flow centerline and exhibits run and tumble dynamics even in the absence of noise.

The paper is structured as follows. In Sec. II, we recall the main results for vesicles. In Sec. III, we show how the equations for a deformable vesicle can be transformed into the equations of a rigid particle in five dimensions. In Sec. IV, we provide exact analytical solutions for vesicles with out-of-plane motion, and thus for the rigid sphere problem. A discussion and a conclusion are presented in Sec. IV.

II. GENERAL ORIENTATION EQUATIONS FOR VESICLES

Here, we recall the main dynamics of vesicles both in the shear plane and out-of-shear plane. Since the vesicle area is fixed, the deformation amplitudes are related [see Eq. (2)] by

$$\frac{\Delta}{2} = 2|F_{22}|^2 + |F_{20}|^2 + 2|F_{21}|^2. \tag{6}$$

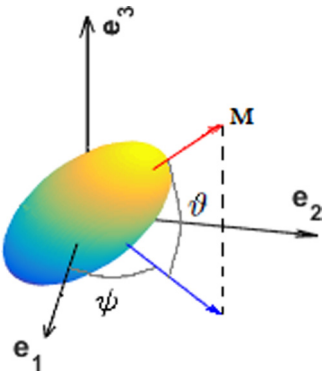

FIG. 1. A schematic view of the vesicle system showing the orientation angle ψ in the shear plane and the angle ϑ measuring deviation out of the shear plane.

If dynamics is restricted to the shear plane, we have $F_{2\pm1} = 0$ (due to the mirror symmetry of the shape in the shear plane, the shape does not contain spherical harmonics of order one), and thus the dynamics is described by the three amplitudes $F_{2\pm2}$ and F_{20} only (instead of five), but only two are independent due to the above constraint. We can introduce the two functions ψ and $\mathcal{R}$, defined by [12]

$$F_{22} = \frac{\sqrt{\Delta}}{2}\mathcal{R}e^{-2i\psi}. \tag{7}$$

With this definition, ψ $(-\pi/2 \leqslant \psi \leqslant \pi/2)$ coincides with the orientation angle of the vesicle main axis, and $0 \leqslant \mathcal{R} \leqslant 1$ is the amplitude of the vesicle deformation. The system of ψ and $\mathcal{R}$ follows from (5):

$$\begin{aligned}\dot\gamma^{-1}\frac{d\mathcal{R}}{dt} &= \chi^{-1}(1-\mathcal{R}^2)\sin(2\psi),\\ \dot\gamma^{-1}\frac{d\psi}{dt} &= -\frac{1}{2}\left(1-\frac{\chi^{-1}}{\mathcal{R}}\cos(2\psi)\right),\end{aligned} \tag{8}$$

which couples vesicle orientation and deformability, with $\chi = \sqrt{\Delta}/2h$. Not surprisingly, this is the system derived for vesicles in [12]. A schematic representation of the meaning of the angle can be found in Fig. 1.

In general, the vesicle is allowed to move outside the shear plane [which is the ($\mathbf{e_1}$-$\mathbf{e_2}$) plane in Fig. 1] and in this case $F_{2\pm1} \neq 0$. As with $F_{2\pm2}$, $F_{2\pm1}$ contains information on the deviation angle outside the shear plane (denoted as ϑ in Fig. 1) and the amplitude of deformation stored in the harmonic $\mathcal{Y}_{21}$. We did not feel it worthwhile to write the equations of motion for ϑ and the amplitude of deformation outside the shear plane, as they will not be used later. Figure 1 shows the angle ϑ of the out-of-shear-plane orientation. The amplitudes $F_{2\pm2}$ and F_{20} describe TT and TB modes while $F_{2\pm1}$ represents the K mode. ϑ is the kayaking angle.

An interesting property that can be obtained from Eq. (5) is that F_{21} obeys

$$\frac{d}{dt}(e^{-it\dot\gamma/2}F_{21}) = \dot\gamma\left\{\frac{4h}{\Delta}\mathrm{Im}(F_{22})e^{-it\dot\gamma/2}F_{21}\right\}. \tag{9}$$

Since F_{20} satisfies

$$\frac{dF_{20}}{dt} = \dot\gamma\frac{4h}{\Delta}\mathrm{Im}(F_{22})F_{20}, \tag{10}$$

one concludes that the new function $e^{-it\dot\gamma/2}F_{21}$ and F_{20} mode satisfy the same equation. This implies, in particular, that

$$\frac{d}{dt}\left(e^{-it\dot\gamma/2}F_{21}F_{20}^{-1}\right) = 0. \tag{11}$$

Therefore, there exists a complex parameter, say D, such that

$$F_{21} = D\left[\cos\frac{\dot\gamma t}{2} + i\sin\frac{\dot\gamma t}{2}\right]F_{20}, \tag{12}$$

showing that the $F_{2\pm1}$ modes can be determined by using the information on F_{20} mode.

III. MAPPING VESICLE EQUATIONS ONTO THOSE OF A RIGID SPHERE IN FIVE DIMENSIONS

This section will focus on the mapping of vesicle equations onto those of a rigid sphere problem. For that purpose, we rewrite Eq. (5) in a vectorial form. We first split the complex amplitudes into real and imaginary parts

$$F_{22} = g_{22} - i\tilde g_{22}, \quad F_{21} = g_{21} + i\tilde g_{21}, \quad F_{20} = \frac{1}{\sqrt{2}}g_{20}, \tag{13}$$

and define a vector $\mathbf{p} \in \mathbb{R}^5$ (containing expansion coefficients of the vesicle shape) by

$$\mathbf{p} = \frac{2}{\sqrt{\Delta}}(g_{22}, \tilde g_{22}, g_{20}, g_{21}, \tilde g_{21}), \tag{14}$$

and a vorticity tensor (dimensionalized by $\dot\gamma$) Ω by

$$\Omega = \begin{pmatrix} 0 & 1 & 0 & 0 & 0\\ -1 & 0 & 0 & 0 & 0\\ 0 & 0 & 0 & 0 & 0\\ 0 & 0 & 0 & 0 & -1/2\\ 0 & 0 & 0 & 1/2 & 0\end{pmatrix}. \tag{15}$$

From the above definitions it can easily be shown that Eq. (5) takes the following form:

$$\dot\gamma^{-1}\frac{d\mathbf{p}}{dt} = \Omega\cdot\mathbf{p} + \chi^{-1}(\mathbf{e}_2 - \mathbf{e}_2\cdot\mathbf{pp}), \tag{16}$$

where $\mathbf{e}_2 = (0, 1, 0, 0, 0)$ and we recall that parameter χ is given by $\chi = \sqrt{\Delta}/2h$, which contains all physical parameters describing the vesicle dynamics in the small deformation theory.

This result shows that vesicle dynamics (at leading order) are completely determined by that of the unit vector $\mathbf{p}$ in $\mathbb{R}^5$ (it can easily be seen that $\mathbf{p}$ is a unit vector). We shall see here that the above vectorial equation is nothing but the equation of a rigid loaded sphere in a gravitational field and subject to a shear flow.

Note, however, that Ω is not the applied vorticity field [which is given, apart from a factor $\frac{1}{2}$, by the first bloc in Eq. (15)] but it corresponds to a fictitious vorticity satisfying (as for the real applied vorticity) $\mathbf{p}\cdot\Omega\cdot\mathbf{p} = 0$ for any vector $\mathbf{p} \in \mathbb{R}^5$ (recall that for any vector $\mathbf{p}$, $\mathbf{p}\cdot\Omega\cdot\mathbf{p} = 0$ if Ω is antisymmetric). The norm of vector $\mathbf{p}$ is preserved since by using (16), we have automatically $\mathbf{p}\cdot d\mathbf{p}/dt = 0$. This agrees with the constraint (6) (normalized vector)

$$p_1^2 + p_2^2 + p_3^2 + p_4^2 + p_5^2 = 1, \tag{17}$$

where $\mathbf{p} = (p_1, p_2, p_3, p_4, p_5)$.

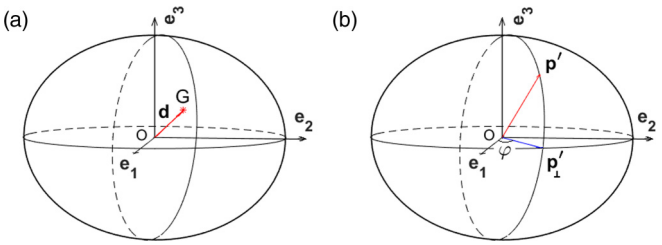

FIG. 2. (a) A schematic view of the loaded particle case in a gravitational field directed along $\mathbf{e_2}$. For a loaded sphere the center of mass G does not coincide with the geometrical center O. The vector $\mathbf{d} = \mathbf{OG}$ represents the loaded direction. The dynamics is described in terms of the unit vector $\mathbf{p}' = \mathbf{d}/d$. (b) The projection of $\mathbf{p}'$ onto the plane $(\mathbf{e}_1, \mathbf{e}_2)$ is denoted as $\mathbf{p}'_\perp$ and it makes angle φ with the $\mathbf{e}_1$ axis.

Actually, the idea of drawing analogy between deformable objects and rigid particles can be found in a work by Omori *et al.* [36], in which a capsule is used as a model for deformable particle (see also a recent paper by Wang *et al.* [37]). In Ref. [36], the authors defined the orientation vector as a unit vector extending from the center of gravity of the capsule to the material point of the membrane located initially at the revolution axis of the unstressed spheroidal capsule. The dynamics of the capsule is determined via the time evolution of the orientation unit vector as a function of the shear rate by using a direct numerical method that combines a finite element method coupled to a boundary integral method as in Ref. [37]. However, the evolution equation of the unit $\mathbf{p}$ is not derived.

In the next section, we start by reviewing some results for vesicles and spherical rigid particles in three dimensions (3D) for reader convenience, before analyzing the mapped equation (16) in five dimensions.

A. A summary of previous studies on loaded rigid sphere in 3D

Here, we briefly report on some well known results obtained for the three-dimensional case. A loaded spherical particle means that the center of mass G does not coincide with the geometrical center O (see Fig. 2). The vector $\mathbf{d} = \mathbf{OG}$ represents the loaded direction. The dynamics is described in terms of the unit vector $\mathbf{p}' = \mathbf{d}/d$. We will see below how to derive the loaded particle dynamics from general and straightforward considerations

First, let us note that the 3D vector $\mathbf{p}' = (p'_1, p'_2, p'_3)$ satisfies an equation similar to Eq. (16) in three dimensions. More precisely, the equation of $\mathbf{p}'$, which is derived from Eq. (16) (by setting the fourth and fifth components to zero), is given by

$$\dot{\gamma}^{-1}\frac{d\mathbf{p}'}{dt} = \Omega' \cdot \mathbf{p}' + \chi^{-1}(\mathbf{e}_2 - \mathbf{e}_2 \cdot \mathbf{p}'\mathbf{p}'), \tag{18}$$

where $\mathbf{e}_2 = (0, 1, 0)$ and

$$\Omega' = \begin{pmatrix} 0 & 1 & 0 \\ -1 & 0 & 0 \\ 0 & 0 & 0 \end{pmatrix}. \tag{19}$$

We have adopted a notation with a prime for both $\mathbf{p}'$ and the vorticity tensor Ω' in order to make a distinction between five dimensions (the mapped problem) and three-dimensional (rigid sphere) equations. Note that in three dimensions $\Omega' \cdot \mathbf{p}'$ can be written as $\omega \times \mathbf{p}'$ (this equivalence does not hold in five dimensions), so that we can also write

$$\dot{\gamma}^{-1}\frac{d\mathbf{p}'}{dt} = \omega \times \mathbf{p}' + \frac{1}{\chi}[\mathbb{I} - \mathbf{p}'\mathbf{p}']\mathbf{e}_2, \tag{20}$$

where ω is the fluid vorticity vector. Note that in 3D Eqs. (20) (for a rigid sphere) and (16) are identical since the vorticity fields Ω and Ω' are the same. We will see that the rigid sphere equations in 5D have exactly the same form as in 3D [i.e., Eq. (20)], in which the vorticity tensor Ω' has to be extended to 5D by taking zero for the new elements. The mapped problem from vesicles still has the same formal equation, however, the vorticity tensor, and is represented by Ω [see Eq. (15)].

Equation (20) accounts for a number of physical applications, as described below. In the next section we will give a simple and general derivation of Eq. (20). Equation (20) was derived for loaded particles in a gravitational field [33] and for polar particles (with a magnetic dipole [34]). In these two cases, $\mathbf{p}'$ is the orientation of the particle. In Eq. (20) parameter χ reads as, respectively (with subscript g for gravity and m for magnetic field),

$$\chi_g = \frac{6\mu\dot{\gamma}}{\rho g d}, \quad \chi_m = \frac{8\pi\mu r_0^3\dot{\gamma}}{q\mathcal{M}}, \tag{21}$$

where ρ is the particle density, μ the fluid viscosity, d the distance between the center of mass and geometrical center, r_0 is the radius of the spherical magnetized particle, $\mathcal{M}$ is the magnitude of the particle's permanent dipole moment, q is the magnitude of the uniform external field vector, and $\mathbf{e}_2 = \mathbf{q}/q$ for the magnetic problem with $\mathbf{q}$ the magnetic field or $\mathbf{e}_2 = \mathbf{g}/g$, where $\mathbf{g}$ is the gravity vector. Parameter χ measures the competition between the shear flow that tends to rotate the particle and the magnetic field (or gravitational field) that tends to orient the particle along the field.

Equation of the type (20) was investigated, independently, in the early papers by Hall and Busenberg [34] and Brenner [33], to understand the effect of an external magnetic field on the viscosity of a dilute suspension of magnetized particles. It has been found that the orientation of an isolated particle depends on χ as well as on the angle $0 \leqslant \Psi \leqslant \pi$ between ω and $\mathbf{j}$. For any $\Psi \neq \pi/2$, Hall and Busenberg [34] have shown by using the Poincaré-Bendixon stability analysis (in two dimensions) and the Stokes' theorem, that orientation $\mathbf{p}'$ tends to the unique stable stationary solution. The case $\Psi = \pi/2$ was also treated by Hall and Busenberg [34] as well as by Brenner [33] independently. It is shown that for $\chi < 1$, orientation $\mathbf{p}'$ tends in time to a certain fixed orientation irrespective of its initial orientation, while for $\chi > 1$, orientation $\mathbf{p}'$ describes one of an infinity family of periodic closed orbits (tumbling motion).

For deformable vesicles in three dimensions (this corresponds to in-plane motion where $F_{2\pm1} = 0$), Eq. (5) [which we know, now, that it is equivalent to Eq. (20) or Eq. (16)] has been numerically [12] and analytically [24] examined. Exact analytical results (see [24]) have determined the regions of the three major types of motions: TT if $\sqrt{\Delta}/2 < h$, or equivalently $\chi < 1$, and TB and VB for $\chi > 1$. The TT to

VB/TB transition occurs at $\chi = 1$ which corresponds to $\Delta = 4h^2$, obtained for vesicles.

Equation (20) is also adopted for microswimmers [35] in the presence of an external flow field. The microswimmer orientation is described by a unit vector $\mathbf{p}'$ and obeys exactly Eq. (20) for appropriate χ as in (21). In addition, one has to specify the motility of the swimmer. This is taken into account by considering that its position $\mathbf{x} \in \mathbb{R}^3$ is described by

$$\frac{d\mathbf{x}}{dt} = \mathbf{u}_0(\mathbf{x}) + \mathbf{v}_s, \tag{22}$$

where $\mathbf{v}_s = v_s\mathbf{p}'$ is the swimming velocity vector relative to the fluid and its magnitude $v_s = |\mathbf{v}_s|$ is assumed to be constant. Equation (22) indicates that the particle velocity is the superposition of the fluid velocity at the particle location $\mathbf{u}_0$ and the swimming velocity $v_s\mathbf{p}'$, where the swimming direction $\mathbf{p}'$ satisfies Eq. (20).

Since the equation of the swimming direction is similar to that of the orientation of vesicles, the dynamics of motile spherical microorganisms bears some resemblance to vesicle dynamics. According to the well known results of vesicle (see [24]), if parameter $\chi > 1$, the particle projection in the xyz space (or vector $\mathbf{p}'$) performs tumbling motion which corresponds to periodic solutions, while if $\chi < 1$, $\mathbf{p}'$ tends to the stable fixed orientation; the swimmer becomes oriented along this final orientation. In other words, Eqs. (20) and (22) account for a run-and-tumble response of the swimming particle upon variation of the parameter χ.

Historically, run and tumbling motions were introduced to describe the dynamics of a class of self-propelled particles such as *E. coli* bacteria [38], which alternate randomly between linear straight runs and circular or reorientation events called tumbles in which the bacterium does not move. Interestingly, Eq. (20) already incorporates run and tumble dynamics via the parameter χ. Thus, an alternative to perform this type of motion would be to attribute to the parameter χ values larger and smaller than unity in a random fashion.

Equations (20) and (22) were used in order to analyze the accumulative behavior of gyrotactic microorganisms (like algae) in a vertical Poiseuille flow [35]. In that study, the authors analyzed only the case where the solution of Eq. (20) is steady (i.e.. $\chi < 1$). We will see below that this equation has exact analytical solutions both steady and time dependent for arbitrary χ. It would thus be interesting in the future to revisit the study presented in [35] in the light of this work. We will say few words on this issue in the section devoted to discussion.

B. Preliminary description in five dimensions

First, Eq. (16) can be explained on the basis of a general consideration. Consider a loaded sphere where $\mathbf{p}'$ is a unit vector joining the geometrical and mass centers (see Fig. 2), in an external gravitational field $\mathbf{e}_2$ (unit vector) and subject to a linear shear flow. Due to the superposition principle in the Stokes regime, one expects the evolution equation to have the form

$$\dot\gamma^{-1}\frac{d\mathbf{p}'}{dt} = \Omega\cdot\mathbf{p}' + \chi^{-1}\mathbf{e}_2. \tag{23}$$

However, this equation does not conserve the norm of $\mathbf{p}'$. To see this, multiply scalarly the equation by $\mathbf{p}'$, one easily sees that $d(\mathbf{p}'^2)/dt \neq 0$ (the first term on the right hand side gives zero but not the second one). In order to enforce the norm of $\mathbf{p}'$, we must supplement Eq. (23) by an additional term

$$\dot\gamma^{-1}\frac{d\mathbf{p}'}{dt} = \Omega\cdot\mathbf{p}' + \chi^{-1}\mathbf{e}_2 + \beta\mathbf{p}', \tag{24}$$

where β is a Lagrange multiplier enforcing the normalization constraint. After a scalar product of the above equation with $\mathbf{p}'$ one sees that $\beta = -\chi^{-1}\mathbf{e}_2\cdot\mathbf{p}'$. Reporting the value of β into Eq. (24) gives Eq. (16) [which is formally identical to Eq. (18); please remember that in 5D Ω', the rigid sphere in 5D, is different from Ω, the mapped problem]. We must keep in mind that Eq. (18) is valid for a rigid sphere at any dimension.

Note that, as in the 3D case, the 5D vector $\mathbf{p}'$ is implicitly introduced here as an orientation vector for the rigid sphere. In fact, in five dimensions $\mathbf{p}'$ can be expressed as

$$\begin{aligned}
p_1' &= \cos\theta_1,\\
p_2' &= \sin\theta_1\cos\theta_2,\\
p_3' &= \sin\theta_1\sin\theta_2\cos\theta_3,\\
p_4' &= \sin\theta_1\sin\theta_2\sin\theta_3\cos\theta_4,\\
p_5' &= \sin\theta_1\sin\theta_2\sin\theta_3\sin\theta_4.
\end{aligned} \tag{25}$$

where $\theta_1,\ \theta_2,\ \theta_3 \in [0,\pi]$ and $\theta_4 \in [0, 2\pi]$. In agreement with our previous notations, we will use the notations $\mathbf{p}$ when referring to the vesicle problem, whereas notation $\mathbf{p}'$ continues to be devoted to the rigid body problem. Let us return to Eq. (16). In order to determine the expression of $\chi = \chi(\Delta, \lambda)$ as a function of physical parameters, of course an explicit solution of the Stokes equations is required.

In order to facilitate a qualitative discussion on the different motions, it is more convenient to cast vectorial equation (16) into the following two systems:

$$\begin{aligned}
\dot\gamma^{-1}\frac{dp_1'}{dt} &= p_2' - \chi^{-1}p_2'p_1',\\
\dot\gamma^{-1}\frac{dp_2'}{dt} &= \chi^{-1} - p_1' - \chi^{-1}p_2'^2,\\
\dot\gamma^{-1}\frac{dp_3'}{dt} &= -\chi^{-1}p_2'p_3'
\end{aligned} \tag{26}$$

and

$$\begin{aligned}
\dot\gamma^{-1}\frac{dp_4'}{dt} &= -\chi^{-1}p_2'p_4' - \frac{1}{2}p_5',\\
\dot\gamma^{-1}\frac{dp_5'}{dt} &= \frac{1}{2}p_4' - \chi^{-1}p_2'p_5'.
\end{aligned} \tag{27}$$

Systems (26) and (27) are decoupled. The first system corresponds, for vesicles, to dynamics in the shear plane (xy), while the second system refers to the out-of-plane dynamics encoded in the amplitudes $F_{2\pm1}$.

According to (7), (13), and (14) we have

$$p_1' = \mathcal{R}\cos(2\psi), \quad p_2' = \mathcal{R}\sin(2\psi). \tag{28}$$

The vesicle equations have been solved exactly when dynamics is restricted to be in the shear plane [24], and will be

recalled below. Note that if the orientation $\mathbf{p}'$ lies in the shear plane, we have $\mathcal{R} = 1$ and then system (8) resembles the KS model for particles of fixed shape:

$$\dot{\gamma}^{-1}\frac{d\varphi}{dt} = -1 + \chi^{-1}\cos(\varphi), \tag{29}$$

which predicts only TT and TB modes, with $\varphi = 2\psi$.

Let us return to Eq. (16). We note that this equation has steady-state solutions depending on parameter χ:

$$\mathbf{p}_{\pm}^{\infty\prime} = \chi\mathbf{e}_1 \pm \sqrt{1-\chi^2}\mathbf{e}_2 \tag{30}$$

for $\chi < 1$, and if $\chi > 1$

$$\mathbf{p}_{\pm}^{o\prime} = \chi^{-1}\mathbf{e}_1 \pm \sqrt{1-\chi^{-2}}\mathbf{e}_3. \tag{31}$$

If $\chi < 1$, the eigenvalues of the matrix associated to the linear part at $\mathbf{p}_{\pm}^{\infty\prime}$, are given by

$$\lambda_1 = \mp\sqrt{\chi^{-2}-1},\ \lambda_2 = \mp 2\sqrt{\chi^{-2}-1},$$
$$\lambda_3 = \mp\sqrt{\chi^{-2}-1} + \frac{1}{2}i,\ \lambda_4 = \mp\sqrt{\chi^{-2}-1} - \frac{1}{2}i,$$

showing that $\mathbf{p}_{+}^{\infty\prime}$ is (asymptotically) stable and $\mathbf{p}_{-}^{\infty\prime}$ is (completely) unstable. That is to say, for $\chi < 1$, the vesicle orientation tends to $\mathbf{p}_{+}^{\infty\prime}$ (TT mode) for large t. The stability analysis shows that at leading order there is no other motion than TT. The TT motion remains stable against out-of-shear-plane perturbation.

If $\chi > 1$, the system is now linearized about $\mathbf{p}_{\pm}^{o\prime}$. The eigenvalues are found to be

$$\lambda_1 = 0, \quad \lambda_2 = \pm i\sqrt{1-\chi^{-2}}, \quad \lambda_3 = \pm i\frac{1}{2}.$$

An eigenvector corresponding to $\lambda_1 = 0$ is given by $\mathbf{e}_3$. Therefore, the vorticity axis is a center for the linearized system. However, nothing can be deduced for the nonlinear system (26) and (27). Below, we investigate general motions by deriving exact expressions of the orientation vector $\mathbf{p}$.

IV. EXACT SOLUTIONS AND DYNAMICS FOR SPHERICAL RIGID PARTICLES

In this section we present exact analytical solutions to the system (26) and (27) aiming to quantify the effect of parameter χ on different vesicle and particle regimes (at leading order).

It is easily seen from system (26) and(27) that for large χ, vorticity becomes important inducing tumbling motion, while for small values of χ the vorticity is neglected allowing the particle to be oriented along $\mathbf{e}_2$.

A. TT-run mode

Exact solutions are first presented for system (26) which constitutes the basic equations in the small deformation theory [12,25]. This system, which is obtained in the case where $F_{2\pm1} = 0$, is solved exactly. The details are explained in [24]. Here, we will extend the analytical solution to the case where $F_{2\pm1} \neq 0$ ($p_4' \neq 0$ and $p_5' \neq 0$).

For $\chi < 1$, the expressions of p_l', $l = 1, 2, 3$, are found to be

$$p_1' = \chi\frac{a\chi^{-2} + \cosh(\Lambda\dot{\gamma}t)}{a + \cosh(\Lambda\dot{\gamma}t)}, \quad p_2' = \chi\Lambda\frac{\sinh(\Lambda\dot{\gamma}t)}{a + \cosh(\Lambda\dot{\gamma}t)},$$
$$p_3' = \Lambda\frac{b}{a + \cosh(\Lambda\dot{\gamma}t)}, \tag{32}$$

which on substituting this result into system (27) gives

$$\dot{\gamma}^{-1}\frac{dp_4'}{dt} = -\frac{1}{2}p_5' - \Lambda\frac{\sinh(\Lambda\dot{\gamma}t)}{a + \cosh(\Lambda\dot{\gamma}t)}p_4',$$
$$\dot{\gamma}^{-1}\frac{dp_5'}{dt} = \frac{1}{2}p_4' - \Lambda\frac{\sinh(\Lambda\dot{\gamma}t)}{a + \cosh(\Lambda\dot{\gamma}t)}p_5'. \tag{33}$$

The general solution of the above linear nonautonomous system is then found to be

$$p_4' = \Lambda\frac{c\cos(\dot{\gamma}t/2) - d\sin(\dot{\gamma}t/2)}{a + \cosh(\Lambda\dot{\gamma}t)},$$
$$p_5' = \Lambda\frac{c\sin(\dot{\gamma}t/2) + d\cos(\dot{\gamma}t/2)}{a + \cosh(\Lambda\dot{\gamma}t)}, \tag{34}$$

by introducing the new function $\tilde{f} = p_4' + ip_5'$, which satisfies

$$\frac{d}{dt}\tilde{f} = \left(-\chi^{-1}p_2' + i\frac{1}{2}\right)\tilde{f}. \tag{35}$$

A simple integration of the above equation leads to (34). In the expressions of $\mathbf{p}'$ parameter Λ is given by

$$\Lambda = \sqrt{|1-\chi^{-2}|}, \tag{36}$$

and a, b, c, and d are real parameters satisfying

$$a^2 + b^2 + c^2 + d^2 = \chi^2. \tag{37}$$

Note that p_4' and p_5' can also be written as

$$p_4' = \Lambda\frac{c_0\cos(\dot{\gamma}t/2 + \theta_0)}{a + \cosh(\Lambda\dot{\gamma}t)}, \quad p_5' = \Lambda\frac{c_0\sin(\dot{\gamma}t/2 + \theta_0)}{a + \cosh(\Lambda\dot{\gamma}t)},$$

for some real θ_0 and c_0 ($a^2 + b^2 + c_0^2 = \chi^2$), so that we may assume in (34) and (37) $d = 0$.

Equations (32) and (34) confirm that the orientation $\mathbf{p}'$ tends to $\mathbf{p}_{+}^{\infty\prime} = \chi\mathbf{e}_1 + \sqrt{1-\chi^2}\mathbf{e}_2$, irrespective of the initial orientation. This corresponds to the (classical) TT motion in which the terminal vector lies (as mentioned before) in the shear plane (in-plane TT). Note that $\mathbf{p}_4'$ and p_5' oscillate and approach 0 as shown in Fig. 3, while the projection of the dynamics into ($\mathbf{e}_1$, $\mathbf{e}_2$, $\mathbf{e}_3$) (the xyz space) tends monotonically to $\mathbf{p}_{+}^{\infty\prime}$.

The orientation angle of the vector $\mathbf{p}'$ (relative to x axis)

$$\varphi(t) = \tan^{-1}\left(\Lambda^{-1}\frac{a\chi^{-2} + \cosh(\Lambda t)}{\sinh(\Lambda t)}\right) \tag{38}$$

tends (monotonically) to

$$\varphi(\infty) = \tan^{-1}(\Lambda^{-1}) = \sin^{-1}(\chi). \tag{39}$$

Finally, we deduce that $\mathcal{R} = \sqrt{p_1'^2 + p_2'^2}$, the particle contour in the shear plane (recall $F_{22} = \sqrt{\Delta}/2\mathcal{R}e^{-2i\psi}$) has the

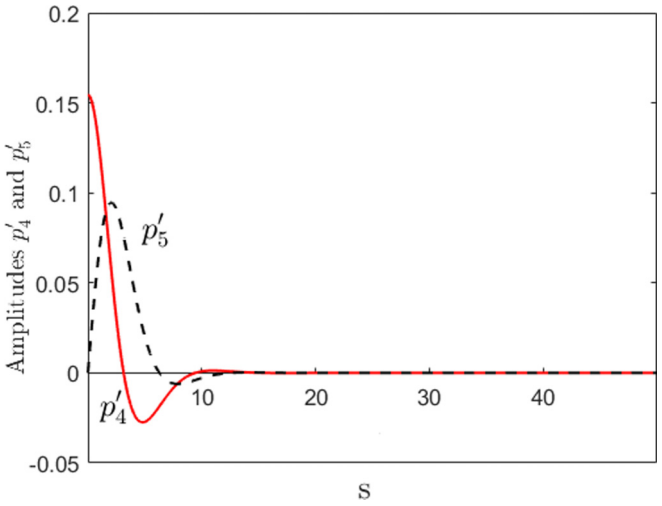

FIG. 3. The dynamics of the components of F_{21} (or equivalently p_4' and p_5') as a function of nondimensional time $s = \dot{\gamma}t$. Parameters are $\chi = 0.4\sqrt{5}$, $a = c = 0.2\sqrt{5}$, and $b = 2\sqrt{0.1}$. Solid (red) line corresponds to the time evolution of p_4' and the time evolution of p_5' is shown in dashed (black) line.

following exact expression:

$$\mathcal{R}^2 = 1 - \frac{(\chi^2 - a^2)\Lambda^2}{[a + \cosh(\Lambda\dot{\gamma}t)]^2}. \tag{40}$$

At long time, $\mathcal{R}$ tends monotonically to 1:

$$\mathcal{R} \approx 1 - \frac{1}{2}(\chi^2 - a^2)\Lambda^2 e^{-2\Lambda\dot{\gamma}t}. \tag{41}$$

Note that if there is no out-of-the-shear-plane deformations (i.e., $F_{20} = 0$ and $F_{2\pm1} = 0$), we have $a = \pm\chi$ and in this case, as is known,

$$\mathcal{R} = 1. \tag{42}$$

Thus, at long time, the orientation vector of the rigid particle will lie in the shear plane and will make an angle $\varphi(\infty) = \sin^{-1}(\chi)$ with $\mathbf{e}_1$ axis. This result shows that the equation of $\mathbf{p}'$ predicts a run motion analogous to TT mode for vesicles for which the orientation angle of the vesicle remains constant.

Our results also show that TT or run mode is accompanied by the oscillations of the $F_{2\pm1}$ modes even if there is no deformation along the vorticity axis. More precisely, $F_{2\pm1}$ modes (or equivalently components $p_4{}'$ and $p_5{}'$) oscillate an infinite number of times through 0 and reach 0 asymptotically for $t \to \infty$, as

$$F_{2\pm1} = C_{\pm}e^{-\sqrt{\chi^{-2}-1}\dot{\gamma}t}\left[\cos\frac{\dot{\gamma}t}{2} \pm i\sin\frac{\dot{\gamma}t}{2}\right]. \tag{43}$$

Figure 3 shows an example of the dynamics of components $p_4{}'$ and $p_5{}'$ which represent cosine shapes with decreasing amplitude.

B. Oscillating modes

We now turn our attention to the time-dependent solutions (which take place for $\chi > 1$). As before, we have only to solve

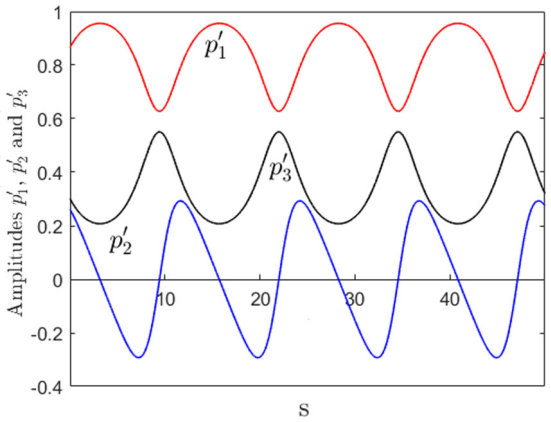

FIG. 4. Evolution of the classical components $\mathbf{p}_l{}'$, $l = 1, 2, 3$, versus nondimensional time $s = \dot{\gamma}t$, for $b = c = 1$ and $\chi = 2/\sqrt{3}$. Parameters $\Gamma = \sqrt{11}/2$ and $a = 2\sqrt{11}/3$ are deduced from (47).

the following linear nonautonomous system for $(p_4{}', p_5{}')$:

$$\dot{\gamma}^{-1}\frac{dp_4'}{dt} = -\frac{1}{2}p_5{}' - \Lambda\frac{\cos(\dot{\gamma}\Lambda t)}{a + \sin(\dot{\gamma}\Lambda t)}p_4',$$
$$\dot{\gamma}^{-1}\frac{dp_5'}{dt} = \frac{1}{2}p_4{}' - \Lambda\frac{\cos(\dot{\gamma}\Lambda t)}{a + \sin(\dot{\gamma}\Lambda t)}p_5', \tag{44}$$

in which we have used system (27) and the exact expression of $p_2{}'$ derived in [24]. More precisely, it is found that components $p_1{}'$, $p_2{}'$, and $p_3{}'$ are given by

$$p_1{}' = \chi\frac{\Gamma + \sin(\dot{\gamma}\Lambda t)}{a + \sin(\dot{\gamma}\Lambda t)}, \quad p_2{}' = \chi\Lambda\frac{\cos(\dot{\gamma}\Lambda t)}{a + \sin(\dot{\gamma}\Lambda t)},$$
$$p_3{}' = \chi^2\Lambda\frac{b}{a + \sin(\dot{\gamma}\Lambda t)}. \tag{45}$$

From (44) one easily deduces that

$$p_4{}' = c\chi^2\Lambda\frac{\cos(\dot{\gamma}t/2)}{a + \sin(\dot{\gamma}\Lambda t)}, \quad p_5{}' = c\chi^2\Lambda\frac{\sin(\dot{\gamma}t/2)}{a + \sin(\dot{\gamma}\Lambda t)}. \tag{46}$$

Here, $a = \Gamma\chi^2$ and Γ, b, and c are arbitrary constants satisfying

$$b^2 + c^2 + \chi^{-2} = \Gamma^2, \tag{47}$$

which guarantees the conservation of the norm of $\mathbf{p}'$. Parameter Λ is given by (36). Note that parameter Γ satisfies $|\Gamma| \geqslant \chi^{-1}$.

Equations (45) and (46) indicate that $\mathbf{p}'$ rotates periodically, as it is shown in Figs. 4 and 5. In the limiting case $|\Gamma| = \chi^{-1}$, one sees from (47) that $b = c = 0$ meaning that orientation $\mathbf{p}'$ oscillates in the shear plane.

C. Where is dynamics of a deformable vesicle hidden in a rigid sphere one?

1. Simplified discussion

A natural question may arise: If dynamics of a deformable object (vesicle) is mapped onto a rigid sphere, where is the deformation hidden? Here, we will discuss this issue. We have recalled in the Introduction that the angle ψ describes the three motions of vesicles (i) TT in which ψ tends to a constant

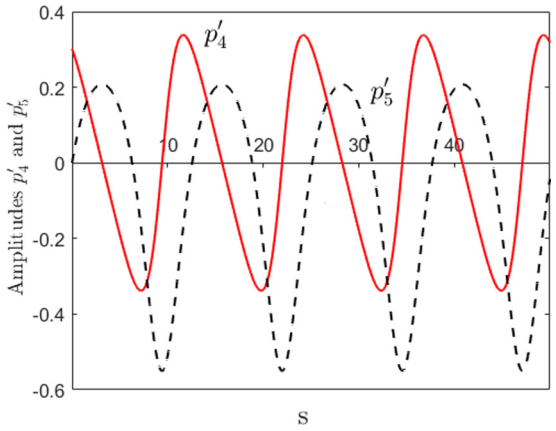

FIG. 5. Components of $p_4{}'$ (solid red line) and $p_5{}'$ (dashed black line) vs nondimensional time $s = \dot{\gamma} t$. Same parameters as in Fig. 4.

value at large time, (ii) TB where the vesicle performs full rotation (the angle oscillates from $-\pi/2$ to $\pi/2$; a rotation by an angle π is a full rotation, since the vesicle is invariant upon a rotation by a such angle), (iii) VB where ψ oscillates between two values (within the interval $[-\pi/4, \pi/4]$).

In order to explain how the rigid body dynamics translates into a deformable particle dynamics, we will need to introduce some preliminaries. For motions of spherical rigid particles, we write (in two dimensions) the projection $\mathbf{p}'_\perp$ of $\mathbf{p}'$ into the shear plane (see Fig. 2) as

$$\mathbf{p}'_\perp = \mathcal{R}\begin{pmatrix}\cos\varphi\\ \sin\varphi\end{pmatrix}, \tag{48}$$

where $\varphi \in (-\pi, \pi]$ is the orientation angle (in the shear plane) that the vector $\mathbf{p}'_\perp$ makes with the $\mathbf{e}_1$ axis. Naturally, $\mathcal{R}$ and φ satisfy a system similar to (8):

$$\begin{aligned}\dot{\gamma}^{-1}\frac{d\mathcal{R}}{dt} &= \chi^{-1}(1-\mathcal{R}^2)\sin(\varphi),\\ \dot{\gamma}^{-1}\frac{d\varphi}{dt} &= -1 + \frac{\chi^{-1}}{\mathcal{R}}\cos(\varphi).\end{aligned} \tag{49}$$

In what follows, we will use angle φ defined in (48). So, the norm of the projected vector $\mathbf{p}'_\perp$ is nothing but $\mathcal{R}$ (the amplitude of deformation) whereas the angle φ is twice the angle that the long axis of the vesicle makes with the flow direction. In other words, following the projection $\mathbf{p}'_\perp$ of the rigid body polarization vector $\mathbf{p}'$ will allow us to understand the correspondence between the two problems. When the projection $\mathbf{p}'_\perp$ has constant orientation in the plane (e_1, e_2), this means that the angle φ is constant and thus we have TT motion for a vesicle. In addition, the norm of $\mathbf{p}'_\perp$ is fixed which means that the deformation amplitude $\mathcal{R}$ is constant. If both $\mathcal{R}$ and the angle φ are constants, this means that the vector $\mathbf{p}'$ has a fixed orientation in 3D. If that vector makes precession around some axis, its projected norm will oscillate in time, and this represents either a VB or a TB in the vesicle problem.

We first consider the case where $F_{2\pm1}(0) = 0$, in which case the dynamics reduces from five to three dimensions. Let us see how dynamics of the vector $\mathbf{p}'$ of the rigid particle problem can be related to the above three modes (TT, VB, and TB). For that purpose, we define $\varphi = \tan^{-1}(p'_2/p'_1)$, which has the exact expressions

$$\varphi(t) = \tan^{-1}\left(\Lambda^{-1}\frac{a\chi^{-2} + \cosh(\Lambda t)}{\sinh(\Lambda t)}\right) \tag{50}$$

for $\chi < 1$, and for $\chi > 1$

$$\varphi(t) = \tan^{-1}\left(\Lambda\frac{\cos(\dot{\gamma}\Lambda t)}{\Gamma + \sin(\dot{\gamma}\Lambda t)}\right). \tag{51}$$

It corresponds to the angle that the projection of $\mathbf{p}'$ (denoted as $\mathbf{p}'_\perp$) into the shear plane makes with the $\mathbf{e}_1$ axis (see Fig. 2). For vesicles, the angle between the long axis and the shear direction is given by

$$\psi = \frac{1}{2}\tan^{-1}\left(\Lambda^{-1}\frac{a\chi^{-2} + \cosh(\Lambda t)}{\sinh(\Lambda t)}\right) \tag{52}$$

and

$$\psi(t) = \frac{1}{2}\tan^{-1}\left(\Lambda\frac{\cos(\dot{\gamma}\Lambda t)}{\Gamma + \sin(\dot{\gamma}\Lambda t)}\right) \tag{53}$$

for $\chi < 1$ and $\chi > 1$, respectively.

Apart from a factor 2, the angle φ for a rigid sphere provides the same information as ψ for a deformable vesicle. This allows us to understand the correspondence between the rigid sphere and the vesicle dynamics. Figure 6 shows a schematic view of the angle φ in the three regimes. Figure 6 shows both the evolution in time of the vector $\mathbf{p}'$ and its projection in the horizontal plane ($\mathbf{p}'_\perp$). In the upper panel we show the case where $\mathbf{p}'$ tends (the red symbol shows the initial condition), after transients, towards a final position whatever the initial position (the solid and dashed lines are issued from different initial conditions). In the heavy bottom spirit, this situation corresponds to the case where the gravity (pointing towards the $\mathbf{e}_2$ direction) is so strong ($\chi < 1$) that the applied shear flow is not capable of making a permanent rotation of the sphere, so that the vector $\mathbf{p}'$ points towards a fixed final direction lying in the horizontal plane. Both the angle φ and the norm of the projected vector $\mathbf{p}'_\perp$ are constant. This corresponds in the vesicle language to the TT mode. When the shear amplitude increases such that χ reaches unity, the shear flow becomes strong enough to overcome the gravity effect. In this case, the shear flow will cause the orientation vector of the heavy bottom sphere to align with the flow direction ($\varphi = 0$). For $\chi > 1$, the shear flow will cause rotation of the vector $\mathbf{p}'$ around some axis (to be specified below). Two cases may happen depending on initial conditions [defined by the constant Γ; see Eq. (47) and discussion below]. The first case is when the vector $\mathbf{p}'$ undergoes precessions without encircling the axis $\mathbf{e}_3$ (red trajectory in Fig. 6). Its projection in the plane $(\mathbf{e}_1, \mathbf{e}_2)$ is elliptic and the norm of $\mathbf{p}'_\perp$ (which represents the deformation amplitude in the vesicle problem) will oscillate in time, whereas the angle φ varies (see more details below) in the interval $[-\pi/2, \pi/2]$ (recall that ψ which the angle between the main axis and the flow direction is half φ). This is the VB mode initially discussed in [12]. The second case corresponds to the situation where $\mathbf{p}'$ undergoes precessions by encircling the axis $\mathbf{e}_3$ (blue trajectory in Fig. 6). The angle φ in this case varies in the interval $[-\pi, \pi]$ (with some oscillations of the norm of $\mathbf{p}'_\perp$), and this corresponds to TB motion.

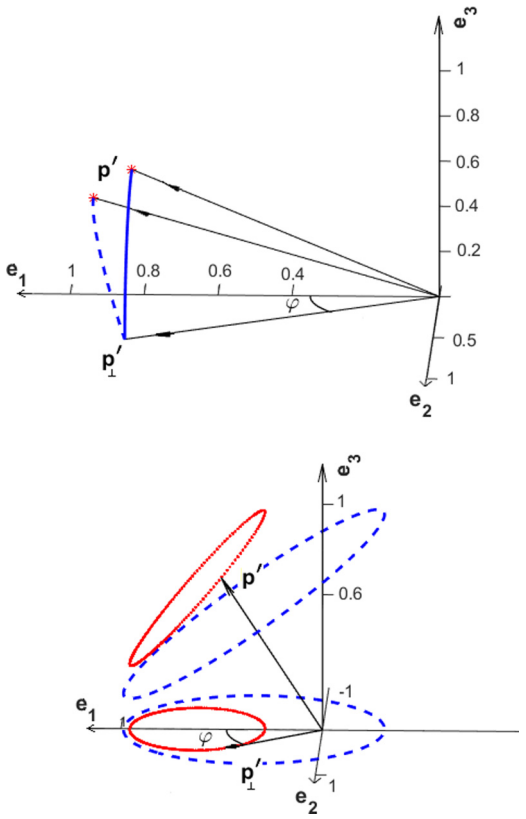

FIG. 6. A schematic view of the evolution of the vector $\mathbf{p}'$ in the course of time, and its projection in the shear plane. Top: the vector tends towards a final orientation (in the shear plane) for $\chi < 1$. The red asterisk represents the initial position. Each initial condition tends towards the same final point. This corresponds to the TT regime for vesicles. Bottom: the vector $\mathbf{p}'$ describes a cone around an axis. The circular inclined trajectory represented by red line (solid line) never goes beyond the vertical axis on the left. Thus, the angle φ oscillates around values which lie in the interval $[-\pi/2, \pi/2]$, corresponding to VB regime. The circular inclined trajectory represented by blue dashed line wraps around the vertical axis on the left. Thus, the angle φ oscillates around values which lie in the interval $[-\pi, \pi]$, corresponding to TB regime; here $\chi > 1$. Whether VB or TB prevails depends on initial conditions. The horizontal red (solid line) and blue (dashed line) trajectories are projections in the $\mathbf{e}_1$-$\mathbf{e}_2$ plane.

2. *Systematic analysis*

In this section, we discuss general solutions of the mapped problem of vesicles. We will then use the notation $\mathbf{p}$ instead of $\mathbf{p}'$ (anyway since the two problems are formally equivalent this should not present any confusion) and refer to system (16). In what follows, we will also use the angle (51) to explore general in-plane motions. As for vesicles, Eq. (51) shows that the time evolution of angle φ is controlled by parameter Γ. We will investigate below the influence of Γ ($|\Gamma| \geqslant \chi^{-1}$), by fixing the parameter χ (and Λ). Recall that Γ satisfies $\Gamma = \pm\sqrt{b^2 + c^2 + \chi^{-2}}$. Without loss of generality we may assume that Γ is positive.

In Fig. 7, we have plotted the time evolution of the orientation angle φ for $\chi = 2/\sqrt{3}$ and three different values of Γ. For $\Gamma < 1$, the particle is in the (classical) tumbling regime. The projection of the orientation axis (into the shear plane) in

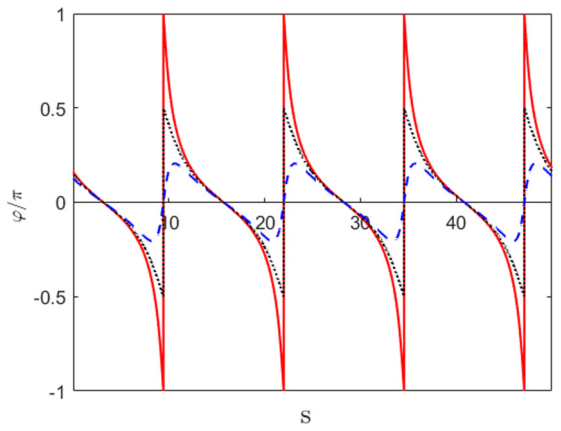

FIG. 7. Dynamics of the orientation angle φ for $\chi := 2/\sqrt{3}$ with $\Gamma = 0.9$ (solid red line) for TB (or KTB), $\Gamma = 1$ (dotted black line), and $\Gamma = 1.2$ (dotted-dashed blue line) for VB (or KBV).

which φ varies from $-\pi$ to π indicates that the particle performs full rotation. For $\Gamma > 1$, we have VB regime. Figure 8 shows the variation of the inclination angle φ as a function of (p_1, p_2) during TB and VB regimes. In the TB regime, the angle undergoes sudden discontinuous jumps in the course of time, whereas in the VB regime the evolution is continuous.

Let us note that from (46), if initially $F_{2\pm1}(0) \neq 0$, then $F_{2\pm1}(t) \neq 0$ for all times. This implies that if initially the main axis of the vesicle is placed off the shear plane, the main axis does not go back to the shear plane. This case which occurs for $\Gamma < 1$, will be called KTB (kayaking-TB).

Note that, as for the classical TB (the TB motion in the shear plane), KTB regime is accompanied with the oscillation of the particle contour in the (xy) plane if $\Gamma \neq \chi^{-1}$, as evidenced by the explicit expression of $\mathcal{R}$:

$$\mathcal{R}^2 = 1 - \chi^4\Lambda^2(\Gamma^2 - \chi^{-2})\frac{1}{[\Gamma\chi^2 + \sin(\Lambda\dot{\gamma}t)]^2}. \qquad (54)$$

The above expression is still valid for all $\chi^{-1} \leqslant \Gamma < \infty$.

For $\Gamma > 1$, Fig. 7 shows that φ oscillates between $\pm\varphi_c$ (with $\varphi_c < \pi/2$). From (51), it is easily deduced that φ_c is

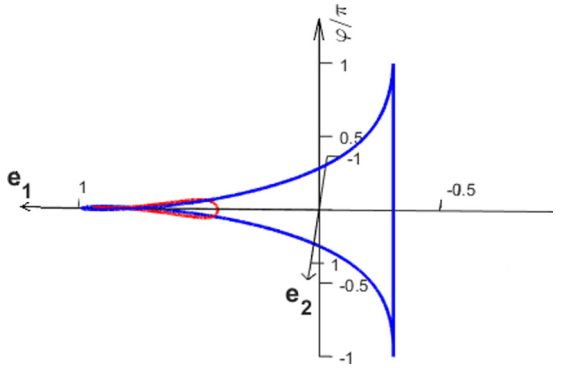

FIG. 8. Evolution of the orientation angle φ as a function of $(\mathbf{p}_1, \mathbf{p}_2)$ during a VB (red) and TB (blue) regime. Parameters are $\Gamma = 0.9$ (TB) and $\Gamma = 1.1$ (VB) and $\chi = 1.25$.

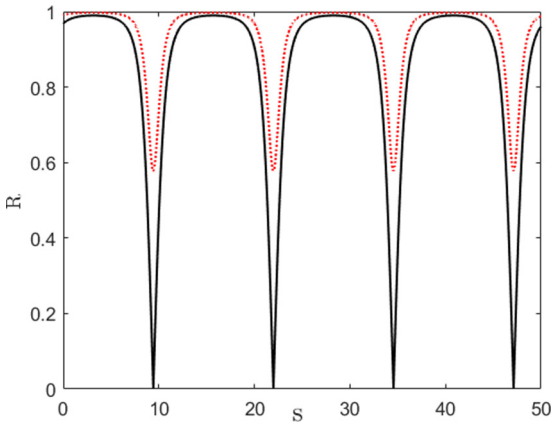

FIG. 9. The behavior of the particle contour in the x-y plane for $\Gamma = 1$ (solid black line) and $\Gamma = 0.9$ (dotted red line).

given by

$$\varphi_c = \tan^{-1}\left(\Lambda \frac{1}{\sqrt{\Gamma^2 - 1}}\right). \tag{55}$$

This regime is also accompanied with the oscillation of $\mathcal{R}$ [see (54)]. The behavior of $\mathcal{R}$ as a function of time is given in Fig. 9 for two different values of Γ. This indicates that the projection of dynamics of a loaded rigid sphere (represented by the unit vector **p**) into the shear plane exhibits a periodic regime which resembles the classical VB regime for deformable particles. The angle φ evolves continuously in the interval $[-\varphi_c, \varphi_c]$ (see Fig. 8). If initially $F_{2\pm1}(0) \neq 0$ the dynamics corresponds to a KVB (kayaking-VB). That is to say, for $\Gamma > 1$, the KTB mode is transformed into the KVB mode.

In Fig. 10, it is shown that orientation vector exhibits different behaviors. Vector **p** does not tend to any fixed orientation, but describes one of an infinite family of closed periodic orbits. In the TT regime (see Fig. 6), the vector **p** tends towards a fixed orientation [given by Eq. (39)] as time elapses. In the VB regime, the vector describes circular trajectories (given by the red circles in Fig. 10). In that case, the projection of the vector in the $\mathbf{e}_1$-$\mathbf{e}_2$ plane oscillates between $\pm\varphi_c$ [Eq. (55)].

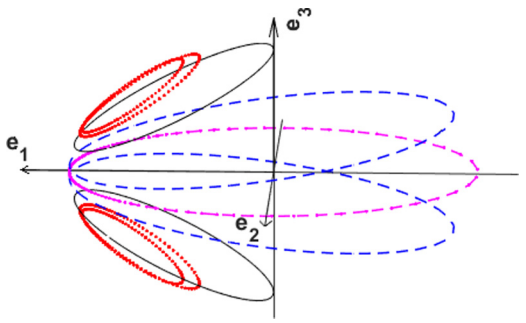

FIG. 10. Different orbits (for 3D) of **p** for different values of parameter Γ. Any selected orbit by a particle is determined by its initial orientation and the given χ. Here, parameter $\chi = 1/0.8$ (and $|\Gamma| \geqslant 0.8$.). Dotted red lines (VB) are obtained for $|\Gamma| > 1$, black lines for $\chi^{-1} < |\Gamma| = 1$ (VB-TB transition), dashed blue line for $0.8 < |\Gamma| < 1$ (TB), and dashed-dotted magenta line for the limiting case $|\Gamma| = 0.8 = \chi^{-1}$.

When $\Gamma = 1$ the VB circular trajectory hits the vertical axis $\mathbf{e}_3$ (black circle). For $\Gamma < 1$ (TB regime), the circular trajectory wraps around the vertical axis (blue circles). The projection of the vector in the $\mathbf{e}_1$-$\mathbf{e}_2$ plane now makes full rotation in that plane.

Finally, it can be checked from the full solution that, during KVB mode, p_1 is always positive and at the KVB-KTB transition p_1 is non-negative and vanishes at finite times. That is to say the KTB-KVB transition is smooth and occurs when the minimum value of the first component of **p** becomes zero over one period. In fact, we may deduce from the exact expressions of **p** that in the KTB-KVB transition, both p_1 and p_2 vanish at the same times (see Fig. 10).

D. Some geometrical properties of the trajectories

In this section we would like to provide some general geometrical properties of the trajectories. In particular, we shall determine the axis of rotation of the trajectories shown in Fig. 10.

By defining $\mathcal{Q} = p_3^2 + p_4^2 + p_5^2$ and by using system (26) and (27), it is easily shown that p_1, p_3, and $\mathcal{Q}$ satisfy the following system of equations:

$$\frac{dp_1}{p_1 - \chi} = \frac{dp_3}{p_3} = \frac{1}{2}\frac{d\mathcal{Q}}{\mathcal{Q}} (= \dot{\gamma}\chi^{-1} p_2 dt). \tag{56}$$

According to the first and third members of the above system, we get the following first integral:

$$\mathcal{H} = \frac{(\chi - \mathbf{p}_1)^2}{p_3^2 + p_4^2 + p_5^2}, \tag{57}$$

which the explicit solutions do not necessarily reveal.

The above first integral is still valid even for $\chi < 1$. In fact, from (57) and the conservation of the norm of **p**, one readily sees that, for some real parameter $\mathcal{C}$,

$$p_1^2 + p_2^2 + \mathcal{C}(\chi - p_1)^2 = 1 \tag{58}$$

or, equivalently,

$$p_2 = \pm\sqrt{1 - p_1^2 + \mathcal{C}(\chi - p_1)^2}, \tag{59}$$

from which we may identify TT, KTB, and KVB depending on parameter $\mathcal{C}$. In particular, for periodic motions, it is more convenient to use parameter $\mathcal{L} (= \pm\mathcal{H}^{1/2})$ given by

$$\mathcal{L} = \pm\frac{\chi - p_1(0)}{\sqrt{1 - p_1^2(0) - p_2^2(0)}}. \tag{60}$$

The above quantity (which is conserved) indicates that if **p** is initially in the shear plane, it remains permanently on that plane ($|\mathcal{H}| = \infty$ for all times).

To extract a relation with the parameter Γ, we use Eqs. (45) at $t = 0$ and (60) to deduce

$$\mathcal{L} = \sqrt{\chi^2 - 1}\frac{\chi\Gamma}{\sqrt{\chi^2\Gamma^2 - 1}}. \tag{61}$$

Here, it is assumed (without loss of generality) that $\mathcal{L} > 0$.

Note that $\mathcal{L}$ takes only values in the interval $(\sqrt{\chi^2 - 1}, \infty)$ (recall that $\Gamma < 1$ corresponds to TB, and $\Gamma > 1$ to VB) and that the particle performs a TB (or KTB) regime if $\mathcal{L} > \chi$, and

a VB (or KVB) regime if $\mathcal{L} < \chi$. The KTB-KVB transition occurs if $\mathcal{L} = \chi$.

As a corollary of the above result, we find that (at leading order) if

$$\chi - p_1(0) > \chi\sqrt{p_3^2(0) + p_4^2(0) + p_5^2(0)}, \tag{62}$$

such that $p_4^2(0) + p_5^2(0) > 0$, we have a KTB regime (which is an out-of-plane TB) in which the angle of the projection of $\mathbf{p}$ into the shear plane (the mean inclination with respect to the flow direction) oscillates in the interval $[-\pi, \pi]$, and components p_4 and p_5 oscillate. If

$$\chi - p_1(0) < \chi\sqrt{p_3^2(0) + p_4^2(0) + p_5^2(0)}, \tag{63}$$

KVB motion takes place, if $p_4^2(0) + p_5^2(0) > 0$, in which the mean inclination angle oscillates in the interval $[-\pi/2, \pi/2]$ accompanied by the oscillations of p_4 and p_5. That is to say, both TB and VB modes exist only if the orientation vector is initially in the shear plane.

According to the above discussion, there exists a (second) critical value $\chi_c > 1$, where KVB ceases to exist and KTB starts. By this we mean that if $1 < \chi < \chi_c$ the loaded rigid sphere exhibits a KTB regime, while if $\chi > \chi_c$ we have a KVB mode, where the critical value χ_c is given by

$$\chi_c = \frac{p_1(0)}{1 - \sqrt{p_3^2(0) + p_4^2(0) + p_5^2(0)}}. \tag{64}$$

To continue our description of motions and their dependence on the initial orientation, we may observe from (45) and (46) that the unit vector $\mathbf{p}$ satisfies

$$\mathbf{p} \cdot (\chi^{-1}\mathbf{e_1} + \tilde{\mathcal{L}}\mathbf{e_3}) = 1, \tag{65}$$

where the (orbit) parameter $\tilde{\mathcal{L}}$ (which is a constant of motion) is defined by the initial orientation of the particle:

$$\tilde{\mathcal{L}} = \frac{\Gamma\Lambda}{b} = \frac{\chi^{-1}\Lambda}{b}\frac{\mathcal{L}}{\sqrt{\mathcal{L}^2 - (\chi^2 - 1)}}. \tag{66}$$

The orientation vector $\mathbf{p}$ then describes a circular cone with the stationary rotation axis with norm 1:

$$\mathbf{k} = (\chi^{-2} + \tilde{\mathcal{L}}^2)^{-1/2}(\chi^{-1}\mathbf{e_1} + \tilde{\mathcal{L}}\mathbf{e_3}). \tag{67}$$

Note that Eq. (67) is still valid in three dimensions and where the rotation axis lies in the (xz) plane, similar to the one shown in Fig. 11.

Similar to parameter $\mathcal{L}$, $\tilde{\mathcal{L}}$ takes only values in a given interval, namely, (Λ, ∞). Two special cases are of interest. For large $\tilde{\mathcal{L}}$ we have $\mathbf{k} = \mathbf{e_3}$. In this limiting case, $p_3 = p_4 = p_5 = 0$. The orbit is exactly the unit circle in the shear plane about the $\mathbf{e_3}$ axis. The second case is obtained if $\tilde{\mathcal{L}} = \Lambda$, which leads to

$$\mathbf{k} = \chi^{-1}\mathbf{e_1} + \sqrt{1 - \chi^{-2}}\mathbf{e_3}. \tag{68}$$

That is to say, rotation axis $\mathbf{k}$ varies between the vorticity axis $\mathbf{e}_3$ and the equilibrium point $\mathbf{p}_+^o$ [see (31)]. This limiting case (68), which occurs for $\Gamma = \infty$, corresponds to a KVB regime with a very small amplitude, according to (55). In fact, as the axis of rotation approaches $\mathbf{p}_+^o$, the KVB amplitude decreases to 0. In addition, by using the exact expression of orientation $\mathbf{p}$ one readily sees that, for large values of Γ, $\mathbf{p}$ approaches $\mathbf{p}_+^o$ and that

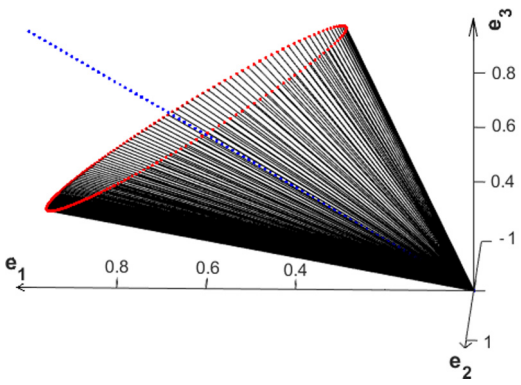

FIG. 11. Typical precession cone of the unit vector $\mathbf{p}$ during a VB mode for the 3D case. The dotted blue line is the fixed central axis of rotation $(\chi^{-1}\mathbf{e_1} + \tilde{\mathcal{L}}\mathbf{e_3})$.

$$p_4 \approx \frac{c\Lambda}{\Gamma}\cos(\dot{\gamma}t/2), \quad p_5 \approx \frac{c\Lambda}{\Gamma}\sin(\dot{\gamma}t/2), \tag{69}$$

in which $c/\Gamma \to 0$. This regime resembles the flow alignment state (as in the swinging regime for capsules [39]). It is an intermediate regime between KVB and TT [22].

V. DISCUSSION AND CONCLUSION

We have shown that the vesicle dynamics in the regime of weak deviation from a sphere (as presented originally in [12]) can be mapped onto dynamics of a loaded rigid sphere (or polar sphere) in a gravitational field in five dimensions. We have then provided exact analytical solutions and have discussed a visual correspondence between the two problems. We have also seen that the evolution equation is used in the context of swimming of microorganisms under gravity and external flow field. In that case, the orientation equation has to be associated with the swimming equation, and the dynamics is described by the system (20) and (22). Depending on χ, the swimmer can perform run ($\chi < 1$) or tumble dynamics ($\chi > 1$). Suppose that the swimmer is placed in a Poiseuille flow and initially located close to the center of the flow. In that vicinity, the shear rate is small enough that χ [given by Eq. (21)] can be made smaller than 1. Then, the swimmer will follow a straight trajectory with a certain angle. When the swimmer is far away from the center, the shear rate tends to be large enough that χ can become larger than one, in which case the swimmer performs TB or VB motions. By preparing different initial random positions and orientations in the flow field, it would be interesting to study the statistics of the spatiotemporal pattern of the swimmers. Since we dispose of an explicit analytical solution of Eq. (20), this task is straightforward. It is hoped to report along this line in the near future.

Here, we have discussed the issue of mapping dynamics of vesicles onto rigid objects in the leading order theory [12]. It would be interesting to investigate if this type of mapping is still valid for other situations. Using the same spirit, a theory of vesicle including cytoskeleton (to mimic RBCs) has been presented [26,40]. How could the mapping work (if any) for this problem is an interesting task for future investigations.

Regarding vesicles, extension of the original theory [12] has been made in order to include higher order deviations from the sphere [16,31,32]. This has resulted in more or less more complicated equations. It is not yet clear whether or not these equations would lend themselves to a simple mapping of the type presented here.

ACKNOWLEDGMENTS

We are grateful to H. Khalfi and H. Fahim for stimulating discussions. This work is supported by CNES (Centre National d'Etudes Spatiale), ESA (European Space Agency), and the French-German University Programme "Living Fluids" (Grant No. CFDA-Q1-14).

[1] P. M. Vlahovska, T. Podgorski, and C. Misbah, C. R. Phys. **10**, 775 (2009).
[2] X. Li, P. M. Vlahovska, and G. E. Karniadakis, Soft Matter **9**, 28 (2013).
[3] P. M. Vlahovska, D. Barthes-Biesel, and C. Misbah, C. R. Phys. **14**, 451 (2013).
[4] D. Abreu, M. Levant, V. Steinberg, and U. Seifert, Adv. Colloid Interface Sci. **208**, 129 (2014), special issue in honor of Wolfgang Helfrich.
[5] S. Keller and R. Skalak, J. Fluid Mech. **120**, 27 (1982).
[6] M. Kraus, W. Wintz, U. Seifert, and R. Lipowsky, Phys. Rev. Lett. **77**, 3685 (1996).
[7] U. Seifert, Phys. Rev. Lett. **83**, 876 (1999).
[8] T. Biben and C. Misbah, Phys. Rev. E **67**, 031908 (2003).
[9] J. Beaucourt, T. Biben, and C. Misbah, Europhys. Lett. **67**, 676 (2004).
[10] H. Noguchi and G. Gompper, Proc. Natl. Acad. Sci. USA **102**, 14159 (2005).
[11] V. Kantsler and V. Steinberg, Phys. Rev. Lett. **95**, 258101 (2005).
[12] C. Misbah, Phys. Rev. Lett. **96**, 028104 (2006).
[13] V. Kantsler and V. Steinberg, Phys. Rev. Lett. **96**, 036001 (2006).
[14] M.-A. Mader, V. Vitkova, M. Abkarian, A. Viallat, and T. Podgorski, Eur. Phys. J. E **19**, 389 (2006).
[15] P. M. Vlahovska and R. S. Gracia, Phys. Rev. E **75**, 016313 (2007).
[16] V. V. Lebedev, K. S. Turitsyn, and S. S. Vergeles, Phys. Rev. Lett. **99**, 218101 (2007).
[17] G. Danker, T. Biben, T. Podgorski, C. Verdier, and C. Misbah, Phys. Rev. E **76**, 041905 (2007).
[18] H. Noguchi and G. Gompper, Phys. Rev. Lett. **98**, 128103 (2007).
[19] V. Lebedev, K. Turitsyn, and S. Vergeles, New J. Phys. **10**, 043044 (2008).
[20] J. Deschamps, V. Kantsler, E. Segre, and V. Steinberg, Proc. Natl. Acad. Sci. USA **106**, 11444 (2009).
[21] A. Farutin, T. Biben, and C. Misbah, Phys. Rev. E **81**, 061904 (2010).
[22] T. Biben, A. Farutin, and C. Misbah, Phys. Rev. E **83**, 031921 (2011).
[23] H. Zhao and E. Shaqfeh, J. Fluid Mech. **674**, 578 (2011).
[24] M. Guedda, M. Abaidi, M. Benlahsen, and C. Misbah, Phys. Rev. E **86**, 051915 (2012).
[25] G. Danker, C. Verdier, and C. Misbah, J. Non-Newtonian Fluid Mech. **152**, 156 (2008).
[26] P. Vlahovska, Y. Young, G. Danker, and C. Misbah, J. Fluid Mech. **678**, 221 (2011).
[27] T. Fischer and R. Korzeniewski, J. Fluid Mech. **736**, 351 (2013).
[28] M. Levant and V. Steinberg, Phys. Rev. E **94**, 062412 (2016).
[29] G. Jeffery, Proc. R. Soc. London A **102**, 161 (1922).
[30] A. P. Spann, H. Zhao, and E. S. G. Shaqfeh, Phys. Fluids **26**, 031902 (2014).
[31] A. Farutin and C. Misbah, Phys. Rev. E **84**, 011902 (2011).
[32] G. Danker and C. Misbah, Phys. Rev. Lett. **98**, 088104 (2007).
[33] H. Brenner, Annu. Rev. Fluid Mech. **2**, 137 (1970).
[34] W. F. Hall and S. N. Busenberg, J. Chem. Phys. **51**, 137 (1969).
[35] T. Pedley and J. Kessler, Proc. R. Soc. London B **231**, 47 (1987).
[36] T. Omori, Y. Imai, T. Yamaguchi, and T. Ishikawa, Phys. Rev. Lett. **108**, 138102 (2012).
[37] Z. Wang, Y. Sui, P. D. M. Spelt, and W. Wang, Phys. Rev. E **88**, 053021 (2013).
[38] H. Berg, *E. coli in Motion* (Springer, New York, 2004).
[39] J. Walter, A.-V. Salsac, and D. Barthès-Biesel, J. Fluid Mech. **676**, 318 (2011).
[40] R. Finken, S. Kessler, and U. Seifert, J. Phys.: Condens. Matter **23**, 184113 (2011).